IEEE Photonics Journal
An IEEE Photonics Society Publication

Open Access

Optical Buffer Device Employing VO_2 Embedded on SOI Waveguides With Microring Resonator

Volume 13, Number 2, April 2021

Lina Fan
Yi Li
Wenqing Zhao
Junxian Li
Xin Zhang
Chuang Peng
Yuda Wu
Mengdi Zou
Baoying Fang
Xiaohua Wang

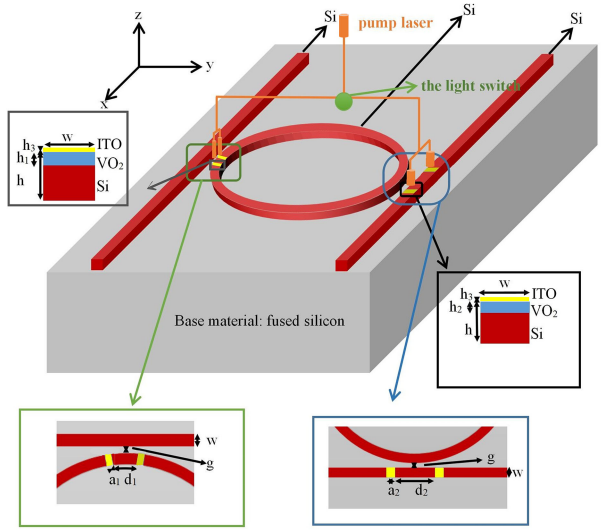

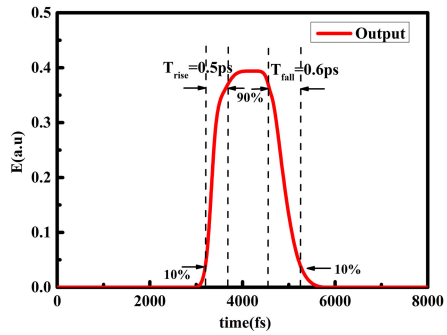

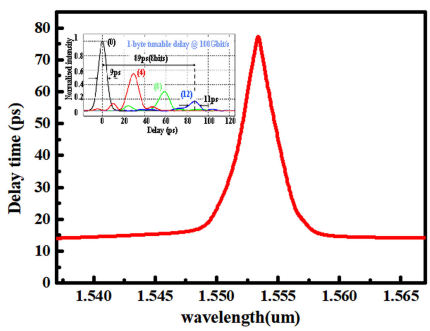

DOI: 10.1109/JPHOT.2021.3057233

Optical Buffer Device Employing VO_2 Embedded on SOI Waveguides With Microring Resonator

Lina Fan,[1] **Yi Li**,[1,2] **Wenqing Zhao**,[1] **Junxian Li**,[1] **Xin Zhang**,[1] **Chuang Peng**,[1] **Yuda Wu**,[1] **Mengdi Zou**,[1] **Baoying Fang**,[1] **and Xiaohua Wang**[1,3]

[1]School of Optical-Electrical and Computer Engineering, University of Shanghai for Science and Technology, Shanghai 200093, China
[2]Shanghai Key Laboratory of Modern Optical System, Shanghai 200093, China
[3]School of Electric and Information, Shanghai University of Electric Power, Shanghai 200090, China

DOI:10.1109/JPHOT.2021.3057233

Manuscript received December 9, 2020; revised January 25, 2021; accepted February 2, 2021. Date of publication February 4, 2021; date of current version March 1, 2021. The work was supported in part by the Key Science and Technology Research Project of Shanghai Committee, China under Grant 10ZZ94 and in part by the Shanghai Talent Leading Plan, China under Grant 2011-026. Corresponding author: Yi Li (e-mail: liyi@usst.edu.cn).

Abstract: Phase-change materials (PCMs) have become as promising elements in silicon photonic systems. We propose an optical buffer device based on vanadium dioxide (VO_2) embedded on silicon-on-insulator waveguides with a microring resonator. The upload straight waveguide is for coupling light signal from the input port into VO_2 embedded on microring resonator and the download straight waveguide with VO_2 films is for coupling the storage signal to the output port. The optical characteristics of optical buffer device under different structural parameters are analyzed by using finite difference mode simulation (MODE). By controlling the phase state of VO_2 in two coupling regions, the buffer speed of the device can be up to 0.5 ps and buffer time up to 78.28 ps. The optical buffer based on VO_2 is a new way for PCM optical buffer.

Index Terms: VO_2, microring resonator, optical buffer.

1. Introduction

In recent years, with the rapid growth of communication data and rapid development of the information industry, people's demand for information processing is increasing. Among them, optical buffer has received extensive attention, and it plays a crucial role in many research fields [1]–[5]. The optical buffer can store optical signals in a short time which can be used in optical storaging [6], optical packet switching [7], all-optical signal processing [8] and etc. It can directly provide optical storage in the optical field without the need for photoelectric conversion, which improves the speed of signal processing and reduces the loss.

At present, the well-known optical buffer design basis mainly includes as following: optical delay effect [9], [10], slow optical effect of optical medium [11]–[15], optical Kerr effect [16], ring resonator coupling [17]–[20] and photonic crystal nanometer effect [21]. Although many studies on optical buffers have been reported, few studies have been reported to achieve high speed optical buffer. In the era of rapid data growth, high speed optical buffering is necessary.

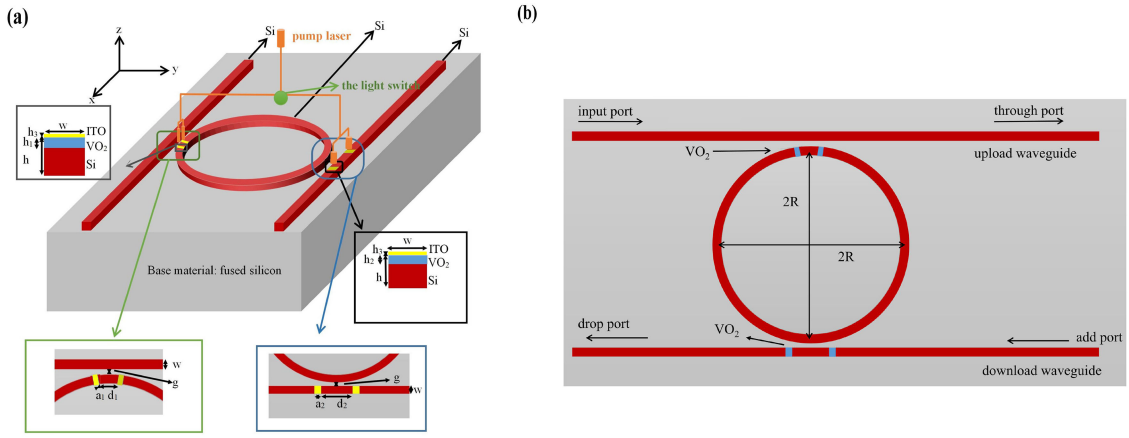

Fig. 1. Optical buffer structure of VO_2-based microring resonator. (a) Schematic diagram of resonator embedded with VO_2 films, the lower illustration is a top view, while the left and right upper corner is the section diagram of VO_2 films on SOI. (b) Microring storage working process.

Some advances have been made in the development of high speed buffer for optical buffer device. In 2014, Jacob Scheuer et al presented a theoretical study of trap door optical buffer based on white light cavity-coupled particle plus/minus filter (ADF) [22]. In 2016, Weilin Liu et al proposed to use the self-pulsating in the active microring resonator as an optical buffer for a nonlinear node in the buffering system, enabling the stored information bits to be written, recovered, reshaping and regenerated at a speed of nanosecond [23]. In 2019, Ajay Kumar et al had achieved high-speed all-optical active low/high state buffer signal processing by using appropriate and effective mixing of microring resonator structures, providing a foundation for high-speed communication and signal processing in the optical field and its switching buffer speed can be up to picosecond [24]. In the same year, Sayed Elshahat et al put forward a five - line (5L) photonic crystal waveguide (PCW) which can realize compact picosecond pulse, optical buffer and low distortion data interconnect. The high buffering performance and low distortion slow light transmission of picosecond pulse are realized [25]. In 2020, Hongkuan Yuan et al reported an all-optical control Terahertz wave storage device based on VO_2 films which demonstrates a 1-bit and 2-bit reconfigurable terahertz wave storage device programmed by two continuous lasers, with storage response time up to microseconds [37]. But as the above surveys show, the research on high speed buffering of optical buffer especially in picosecond speed is still insufficient.

In this paper, we propose an optical buffer device based on VO_2 films embedded on silicon on insulator (SOI) waveguide microring resonator due to phase transition characteristics of VO_2. As we all know, the phase transition of VO_2 is essentially the transition of electrons, while the change of carrier density is the main reason for the orderly change, and the mobility is only affected by two factors [26]. Therefore, due to the variation of free carrier density, its dielectric properties, refractive index [27]–[29] and extinction parameters are highly adjustable, providing conditions for many photonic applications and especially in optical buffering. This device combines VO_2 films with existing silicon waveguide technologies to realize optical buffer, which can not only improve the storage speed and greatly reduce the size of devices but also promote the new aspect of VO_2 application in silicon waveguide.

2. Device Structure and Principle

Here, we propose an integrated optical buffer device based on VO_2 films and analyze the main principle of device. Fig. 1 shows the schematic cross section of the optical buffer device, which consists of one upload straight silicon waveguide, one download straight silicon waveguide embedded two

rectangular VO_2 films in the coupling region and one microring silicon waveguide embedded two arc VO_2 films in the coupling region between the upload waveguide and the ring waveguide on fused silicon substrate. The upload straight silicon waveguide is for coupling the light signal from the input port into the microring and the download straight silicon waveguide is for coupling the light signal from the microring to the drop port. The width and thickness of the straight silicon waveguide and the ring silicon waveguide are the same, which are respectively w and h as shown in Fig. 1(a). The radius of the ring waveguide and the arc length of VO_2 films are R and a_1, respectively. The spacing between the ring waveguide and two straight waveguides is g. The depth of two arc VO_2 films embedded in the ring waveguide is h_1 and the distance between them is d_1. Similarly, the depth of two rectangular VO_2 films embedded in the download straight waveguide is h_2, and the distance between them and the length of VO_2 films are d_2 and a_2, respectively. To prevent VO_2 films from being oxidized, thin ITO films with a thickness of $h_3 = 50$ nm are coated on its surface. ITO films are optically transparent throughout the visible spectrum, therefore, plating ITO on VO_2 will not have a great impact on the transmission of light [39].

In order to prepare the designed optical buffer, the following steps are required. Firstly, the straight waveguide and ring waveguide are fabricated by the standard SOI process. Secondly, photolithography and etching are used to open the windows for VO_2 films in the region of ring waveguide and download straight waveguide. Then, the VO_2 films can be prepared in the etched area by coating. Finally, a layer of ITO is deposited on the VO_2 films in the way of vaporization deposition and the designed optical buffer can be made. The storage and reading of device can be realized by controlling the embedded VO_2 films phase transition states. As shown in Fig. 1(a), We inject the pump laser with $\mathbf{1} \times \mathbf{2}$ beam splitter and switch light onto the embedded VO_2 films to induce a photoinduced phase change. The switching time of optical switch can be on the order of femtosecond [42] which does not affect the storage and read of device. In 2008, M. Rini et al elaborated the luminous fluence of VO_2 films photoinduced phase transition is 250 μJ/cm^2 [34]. When the injected laser fluence is less than 250 μJ/cm^2, VO_2 is in the insulating state, otherwise VO_2 is in the metallic state, comparable to but less than the optical fluence needed to initiate refractive index changes in silicon (of order 1–2 mJ/cm^2) [34]–[36], which shows that the externally controlled laser will not affect the Si waveguide channel transmission.

When the light signal enters the upload straight waveguide from the input port, one part of the light is coupled into the ring waveguide, and the other part is output directly through the upload waveguide as shown in Fig. 1(b). The different phase states of the embedded VO_2 films controlled by the pump laser will affect the coupling coefficient in the coupling region and the mode distribution of the waveguide. By selecting the appropriate structural parameters, the light signal of the upload waveguide can be fully coupled and stored in the ring waveguide, and the light signal stored in the ring waveguide can be read by the download waveguide. Fig. 2 shows the optical energy wave amplitudes guided in the input, through, add and drop ports are respectively denoted as E_{input}, E_1, E_{add}, E_3. When VO_2 films embedded in the ring waveguide are in the insulating state (U-VO_2-I) and the films embedded in the download straight waveguide are in the metallic state (D-VO_2-M) controlled by pump laser, the coupling between the waveguides in coupling region 1 is strong and in the coupling region 2 is weak, then the light signal can be written into the ring waveguide. At the end of the optical information writing, the pump laser is injected to make the VO_2 films embedded in the ring waveguide change to a metallic state (U-VO_2-M) which makes the coupling in coupling region 1 weak, preventing the light continuing to input into the ring waveguide. If the light signal stored in the ring waveguide is to be read out, the pump laser is removed to make the VO_2 films embedded in the download straight waveguide transform into an insulating state (D-VO_2-I). The coupling enhancement of coupling region 2 can make the light signal in the ring waveguide be coupled and read out from the drop port.

Fig. 2 shows the structure parameters of device in coupling regions. According to the microring resonator's coupling theory [40] and oscillator model [41], in the coupling region 1 between the upload waveguide and the ring waveguide, the amplitude coupling coefficients and transmission coefficients are k_{21}, k_{12}, m_1, respectively, which can be calculated by formula (1) and (2), where

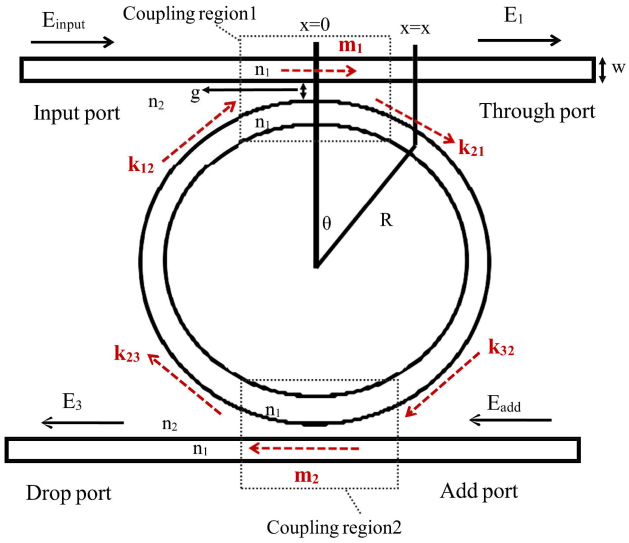

Fig. 2. A schematic diagram of silicon microring storage.

$\gamma_{11}{}^2 = k_0{}^2 n_1{}^2 - \beta_1{}^2$, $\gamma_{21}{}^2 = \beta_1{}^2 - k_0{}^2 n_2{}^2$, and $\beta_1 = k_0 n_{eff1}$ is the propagation constant;

$$k_{21} = k_{12} = sin\left[R\int_{-\frac{\pi}{2}}^{\frac{\pi}{2}} \frac{\gamma_{11}{}^2\gamma_{21}{}^2}{\beta_1 * k_0{}^2(n_1{}^2 - n_2{}^2)(1+\gamma_{21}w/2)} exp[\gamma_{21}(g+R-Rcos\theta)]\,cos^2\theta\, d\theta\right] \quad (1)$$

$$m_1 = cos\left[R\int_{-\frac{\pi}{2}}^{\frac{\pi}{2}} \frac{\gamma_{11}{}^2\gamma_{21}{}^2}{\beta_1 * k_0{}^2(n_1{}^2 - n_2{}^2)(1+\gamma_{21}w/2)} exp[\gamma_{21}(g+R-Rcos\theta)]\,cos^2\theta\, d\theta\right] \quad (2)$$

$k_0 = 2\pi/\lambda_0$ is the wave number in vacuum; λ_0 is the input wavelength; n_{eff1} is the effective refractive index of light wave in the waveguide which depends on w, h, a_1, d_1, h_1, R and n_1; n_1 and n_2 are the refractive index of silicon and the air, respectively; θ is the coupling angle between the two waveguides at x position.

In the coupling region 2 between the download waveguide and the ring waveguide, the amplitude coupling coefficients and transmission coefficients are k_{23}, k_{32}, m_2, respectively, which can be calculated by formula (3) and (4),

$$k_{32} = k_{23} = sin\left[R\int_{-\frac{\pi}{2}}^{\frac{\pi}{2}} \frac{\gamma_{12}{}^2\gamma_{22}{}^2}{\beta_2 * k_0{}^2(n_1{}^2 - n_2{}^2)(1+\gamma_{22}w/2)} exp[\gamma_{22}(g+R-Rcos\theta)]\,cos^2\theta\, d\theta\right] \quad (3)$$

$$m_2 = cos\left[R\int_{-\frac{\pi}{2}}^{\frac{\pi}{2}} \frac{\gamma_{12}{}^2\gamma_{22}{}^2}{\beta_2 * k_0{}^2(n_1{}^2 - n_2{}^2)(1+\gamma_{22}w/2)} exp[\gamma_{22}(g+R-Rcos\theta)]\,cos^2\theta\, d\theta\right] \quad (4)$$

where $\gamma_{12}{}^2 = k_0{}^2 n_1{}^2 - \beta_2{}^2$, $\gamma_{22}{}^2 = \beta_2{}^2 - k_0{}^2 n_2{}^2$, $\beta_2 = k_0 n_{eff2}$, n_{eff2} depends on w, h, a_2, d_2, h_2, R and n_1. The coupling coefficient determines the coupling efficiency of device. The transmission to the through port and drop port can be respectively derived as formula (5) and formula (6). The formula (7) calculates the phase φ, where φ is phase change; φ_1 and φ_2 respectively represent the light passes through the phase change of two half regions; n_{eff} is the effective refractive index of the ring waveguide; γ is the attenuation factor for the transmission of light in a ring cavity, which is related to the length of the coupling region, a_1, d_1 and h_1.

$$E_1 = \frac{m_1 - m_2\gamma\, exp(-j\varphi)}{1 - m_1 m_2\gamma\, exp(-j\varphi)} E_{input} + \frac{-k_{21}{}^2\gamma_2 exp(-j\varphi_2)}{1 - m_1 m_2\gamma\, exp(-j\varphi)} E_{add} \quad (5)$$

$$E_3 = \frac{-m_1 m_2 \gamma_1 exp(-j\varphi_1)}{1 - m_1 m_2 \gamma exp(-j\varphi)} E_{input} + \frac{m_2 - m_1 \gamma exp(-j\varphi)}{1 - m_1 m_2 \gamma exp(-j\varphi)} E_{add} \quad (6)$$

$$\varphi = \beta 2\pi R = \frac{2\pi}{\lambda_0} n_{eff} 2\pi R \quad (7)$$

Due to the small photoelectric coefficient in silicon and the limitation of carrier life of injected silicon based devices, there are some effects on storage speed and buffer time of all-silicon optical buffer, which can be solved by using optically pumped hybrid Si-VO_2 ring resonators. When the device is embedded with VO_2 films, the effective refractive index of coupling regions can be adjusted to control the coupling coefficient of device, realizing the control of input light and improving the performance of device. Fig. 3(a)–3(b) respectively show the relationship between w and n_{eff} in coupling region 1 and 2 with and without the embedded VO_2 films, where the n_{eff} in coupling region 1 and 2 with the embedded U-VO_2-M and D-VO_2-M is significantly greater than that without the embedded VO_2 films. Similarly, the relationship between h and n_{eff} is shown in Fig. 3(c)–3(d) that the change trend is the same as that in Fig. 3(a). The w and h of the waveguide can't be too large which will support higher order modes and degrade the performance of the microring storage, so we selected $w = 0.4$ μm and $h = 0.18$ μm. In addition, we choose $g = 0.1$ μm as the device parameter for satisfying coupling efficiency and preparation process. Considering the n_{eff} of the ring waveguide and the appropriate device size, the waveguide radius selected in this paper is $R = 3.1$ μm.

Based on the selection of device parameters w, h, R and g, Fig. 3(e) shows the extinction ratio in the drop port of device with and without the embedded U-VO_2-I and D-VO_2-M, where $ER = 10log_{10}[\frac{(T_d)_{max}}{(T_d)_{min}}]$. With the embedded VO_2 films, the ER is sacrificed to realize the storage performance, and the maximum ER is 16.82 dB at $\lambda = 1.5537$ μm. At the same time, Fig. 3(f) shows the relationship between the coupling angle θ of coupling region 1 and n_{eff} in the device embedded with VO_2 films, the n_{eff} increases with the θ increasing. The coupling length is related to θ. Fig. 3(g) shows the relationship between coupling length and coupling efficiency. The coupling efficiency increases first and then decreases with the increase of coupling length.

When the device is in the writing state in coupling region 1, Fig. 4(a)–4(c) show the transmissions of through port and drop port change with a_1, d_1, h_1, respectively. Fig. 4(a) shows that the transmission in the drop port decreases with the increase of a_1 while the transmission in the through port increases. In order to achieve better storage function, we select $a_1 = 0.16$ μm. Fig. 4(c)–4(f) have the same change trend as Fig. 4(a). When the device is in the writing state in coupling region 2, Fig. 4(d)–4(f) show the transmissions of through port and drop port change with a_2, d_2, h_2, respectively. Finally we select $h_1 = 0.03$ μm, $a_2 = 0.32$ μm, $d_2 = 2.4$ μm and $h_2 = 0.03$ μm. Fig. 4(b) demonstrates the transmissions of drop port and through port are minimum at $d_1 = 0.757$ μm.

In conclusion, according to the above analysis, the optimized device structure parameters are as following: the height of the straight waveguide is $h = 0.18$ μm and the width of it is $w = 0.4$ μm; The radius of the ring waveguide is $R = 3.1$ μm; The gap between the straight waveguide and the ring waveguide is $g = 0.1$ μm; The distances between the VO_2 films embedded in the ring waveguide and the download straight waveguide are respectively $d_1 = 0.757$ μm and $d_2 = 2.4$ μm; The lengths of VO_2 films are respectively $a_1 = 0.16$ μm and $a_2 = 0.32$ μm; The depths of the VO_2 films are $h_1 = h_2 = 0.03$ μm.

3. Optical Buffer Performance Analysis

We use the finite-difference model (MODE) and coupled mode-theory(CMT) [30] to simulate and analyze the device performance. In order to obtain the optimal results, we use varFDTD (finite-difference time-domain) method to set the perfectly matched layer (PML) boundary conditions along the x and y directions and metal boundary conditions along the z direction. The mode of light pulse used is TE mode since this kind of mode loss is relatively low. At the same time, the optical pulse

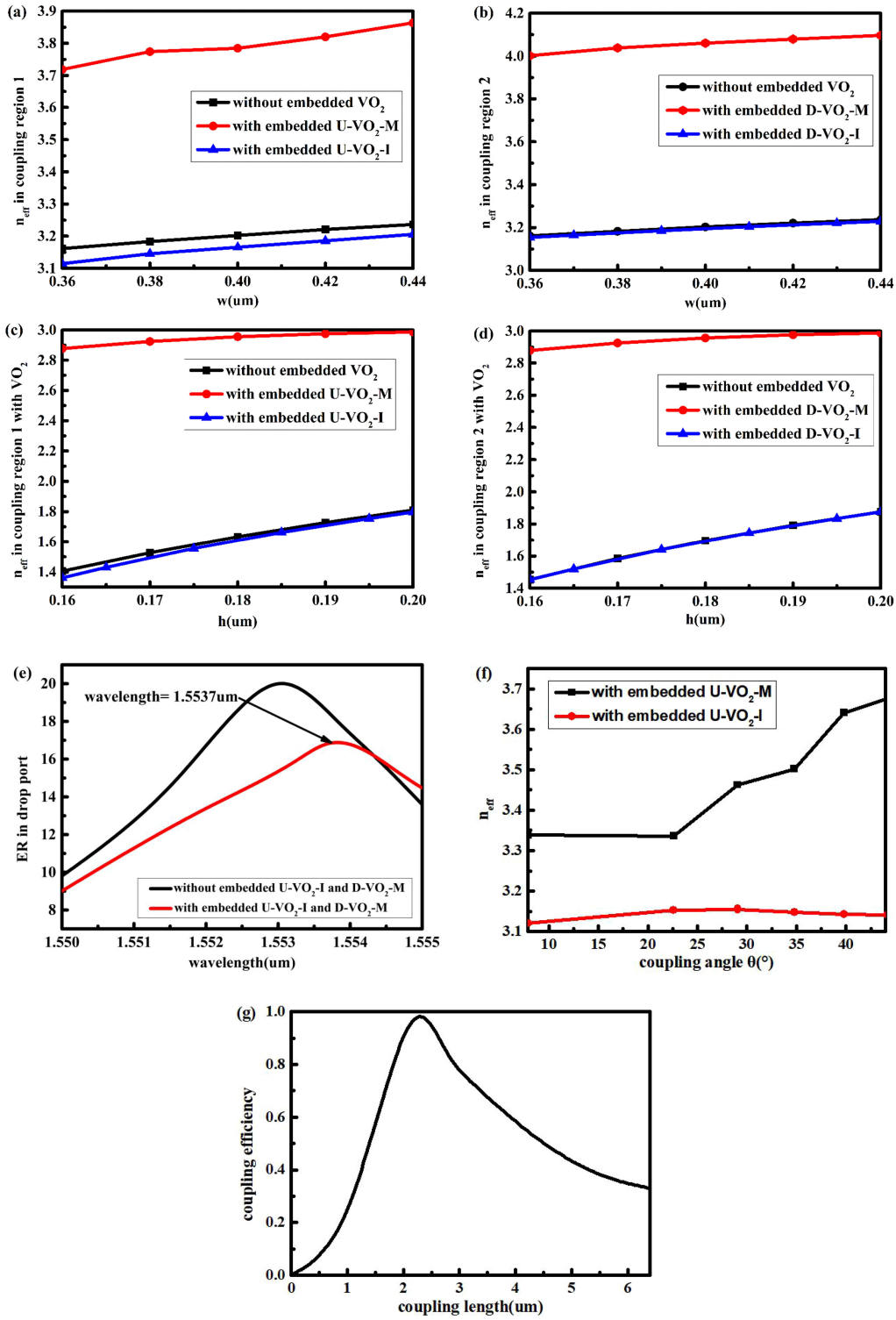

Fig. 3. Parameter optimization of devices. (a) - (b) The relationship between w and n_{eff} in coupling region 1 and 2 with and without the embedded VO_2 films. (c) - (d) The relationship between h and n_{eff} in coupling region 1 and 2 with and without the embedded VO_2 films. (e) Extinction ratio (ER) of the device's drop port with and without the embedded U-VO_2-I and D-VO_2-M. (f) The relationship between θ and n_{eff} in coupling region 1 with the embedded VO_2 films. (g) The relationship between coupling length and coupling efficiency.

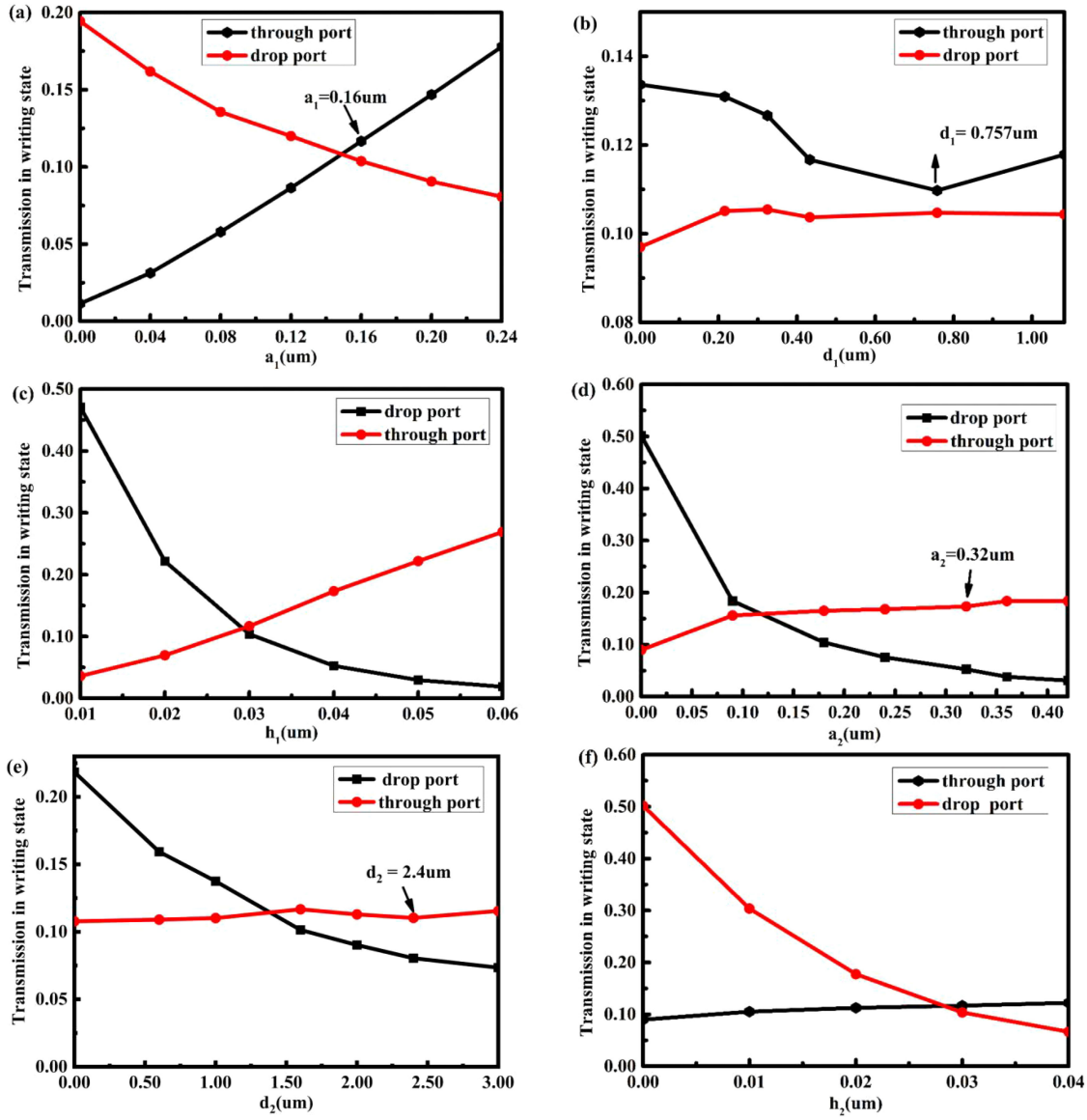

Fig. 4. Parameter optimization of the embedded VO_2 films when the device is in the writing state. (a) - (f) The transmissions of through port and drop port change with a_1, d_1, h_1, a_2, d_2, h_2, respectively.

is incident to the structure along the positive direction of the *x*-axis, and the power monitor [31] is used to calculate the transmission and electric field distribution. The mesh precision used is 1/14 of the wavelength. When the MODE method is adopted for simulation, the fused silicon data comes from Palik database, and the refractive index data of VO_2 comes from Refs. [32], [33].

It can be seen in Fig. 5, the propagation of light signal in the microring buffer is different before and after the VO_2 phase transition in coupling region 1 and 2. Fig. 5(a)–5(b) respectively show the electric field distribution when the device realizes the writing and reading functions. When the device realizes the writing function, the input light signal is stored in the ring waveguide then the device through port and drop port have almost no light signal output which can be seen in Fig. 5(a). At the same time, the transmissions of device through port and drop port are almost zero in Fig. 5(c) and the signal stored in the ring waveguide is shown in Fig. 5(e). When the device realizes the reading function, the light signal can be read from the ring waveguide to the drop port

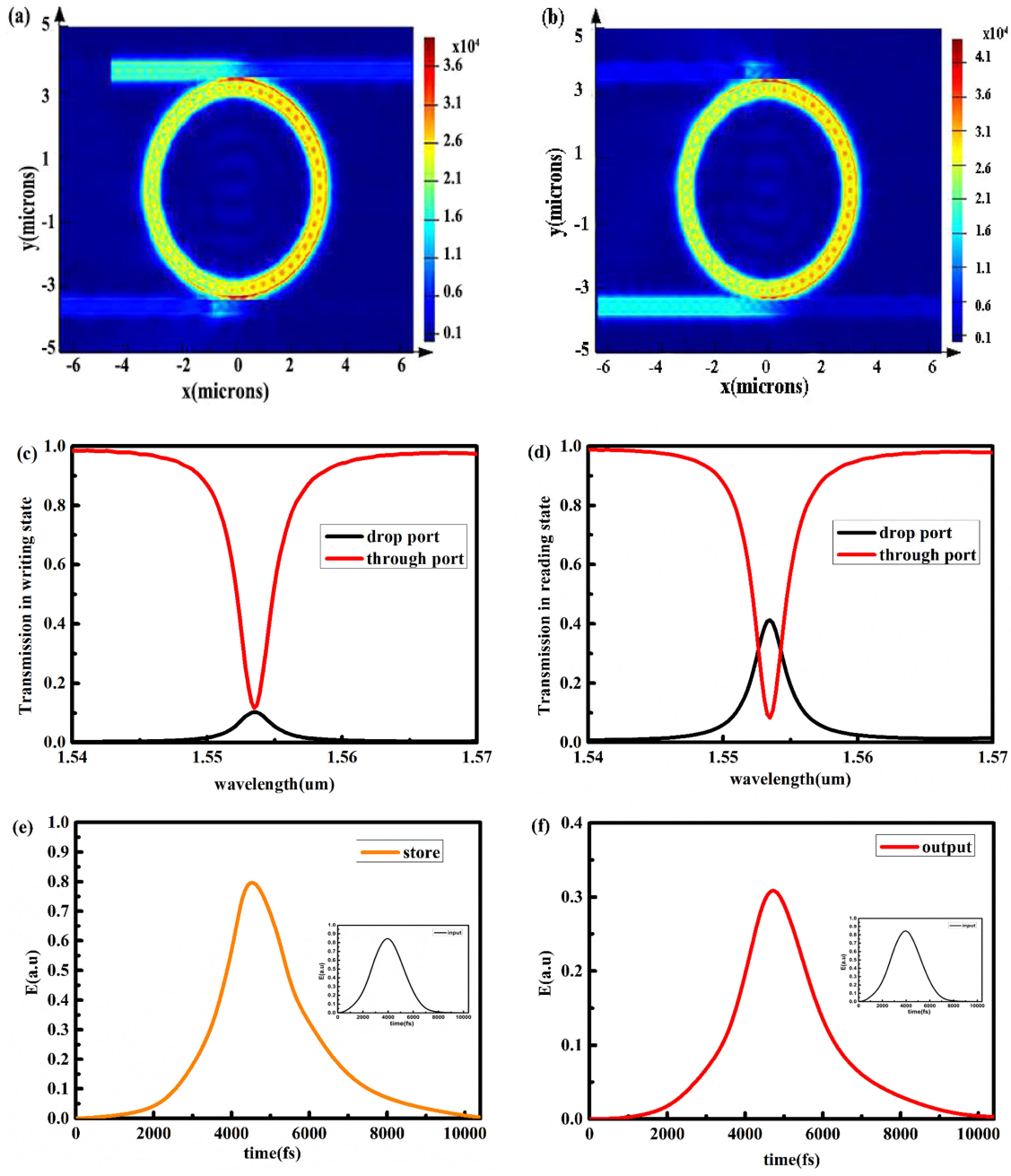

Fig. 5. (a) - (b) The electric field distributions of the microring storage in the writing and reading state. (c) - (d) The transmissions of device in the writing and reading state. (e) Stored signal, the illustration is the input signal. (f) Output signal.

as shown in Fig. 5(b). Meanwhile, Fig. 5(d) shows the transmissions of device through port and drop port that the light signal stored in the ring waveguide is all coupled and read out from the drop port, and the signal output from drop port is shown in Fig. 5(f). At the same time, it can be obtained that the propagation loss of the ring resonator is 2.9×10^{-5} dB/μm and the propagation loss of the section with insulating state VO_2 films is 0.43 dB/μm. The propagation loss of the section with metallic state VO_2 films is 4.63 dB/μm. The microring Q-factor is 545.473.

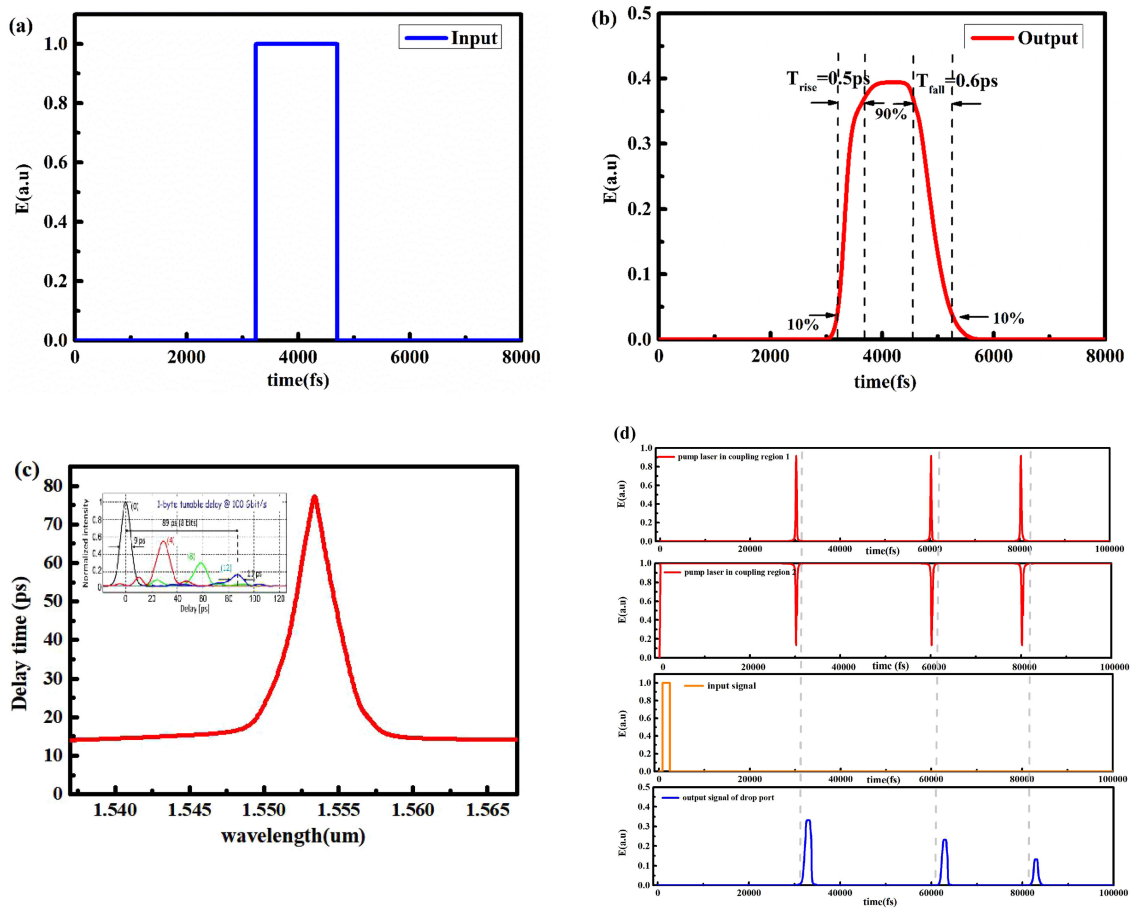

Fig. 6. (a) Input pulse signal. (b) Output optical signal with rise/fall time of 0.5 ps / 0.6 ps. (c) Delay time and wavelength, Illustrations is from Ref. [38]. (d) The relationship between the external pump laser pulse, the input signal and the output signal of drop port.

In order to describe the speed response of the optical buffer, a picosecond pulse drive signal is added to the input port of device. The pulse length of the input signal is 1.6 ps as shown in Fig. 6(a). The phase transition speed of VO_2 films with thickness of 50 nm and area of 1 μm^2 under 250 $\mu J/cm^2$ pump laser at a wavelength of 800 nm can reach at femtosecond as reference [34], [35] shows. The thickness and area of VO_2 films in this paper are less than that of VO_2 films in reference [34],[35], thus the phase transition speed of VO_2 films in this paper can also reach the order of femtosecond under 250 $\mu J/cm^2$ pump laser at a wavelength of 800 nm. Then Fig. 6(b) shows the output signal of the drop port where rise and fall time are respectively 0.5 ps / 0.6 ps that are faster than the Sayed Elshahat's research [25]. The insertion loss of the optical buffer device is about 6.54 dB when inputting a 1.5537 μm light pulse, including the coupling loss between the straight waveguide and the ring waveguide and the insertion loss of VO_2 films in coupling region 1 and 2. Fig. 6(c) shows the relation between wavelength and delay time. The maximum delay time of the buffer device is 78.28 ps at $\lambda = 1.5537$ μm, which is similarly to group delay time of coupled resonator optical waveguides (CROWs) with 8$\sim$12 open rings [38]. At the same time, Fig. 6(d) shows the relationship between the external pump laser pulse, the input signal and the output signal of drop port. The output signal of the drop port can be obtained by controlling the phase state of VO_2 films with an external pump laser. With the increase of buffering time, the amplitude of output signal of drop port decreases continuously.

4. Conclusion

In conclusion, the optical buffer device employing VO_2 embedded on SOI waveguides with micro-ring resonator is analyzed by varFDTD method. By injecting certain energy pump laser to respectively control the phase state of the embedded VO_2 films in coupling region 1 and 2, enabling the device to respectively achieve writing, storaging and reading functions. The ER of device is up to 16.82 dB and the buffer speed can reach 0.5 ps. Buffer time can reach 78.28 ps. Our results prove that VO_2 can be combined with waveguide devices to realize the function of optical storage which has sub-picosecond storage speed, high ER and smaller device's size. It can be seen that our results are an important step towards broad, fast, low-power on-chip photons and promote the development of optical buffer.

Acknowledgment

The authors would like to thank Professor Li Yi for his careful guidance.

References

[1] E. F. Burmeister, D. J. Blumenthal, and J. E. Bowers, "A comparison of optical buffering technologies," *Opt. Switching Netw.*, vol. 5, no. 1, pp. 10–18, 2008.
[2] X. Wang *et al.*, "Continuously tunable ultra-thin silicon waveguide optical delay line," *Optica*, vol. 4, no. 5, pp. 507–515, 2017.
[3] H. J. Dorren, N. Calabretta, and O. Raz, "Scaling all-optical packet routers: How much buffering is required? [Invited]," *J. Opt. Netw.*, vol. 7, no. 11, pp. 936–946, 2008.
[4] J. T. Mok and B. J. Eggleton, "Photonics: Expect more delays," *Nature*, vol. 433, no. 7028, pp. 811–812, 2005.
[5] F. Xia, L. Sekaric, and Y. Vlasov, "Ultracompact optical buffers on a silicon chip," *Nat. Photon.*, vol. 1, no. 1, pp. 65–71, 2007.
[6] L. Tancevski, L. Tamil, and F. Callegati, "Nondegenerate buffers: An approach for building large optical memories," *IEEE Photon. Technol. Lett.*, vol. 11, no.no. 8, pp. 1072–1074, Aug. 1999.
[7] T. Tanemura *et al.*, "Large-capacity compact optical buffer based on InP integrated phased-array switch and coiled fiber delay lines," *J. Lightw. Technol.*, vol. 29, no. 4, pp. 396–402, 2010.
[8] A. E. Willner, S. Khaleghi, M. R. Chitgarha, and O. F. Yilmaz, "All-optical signal processing," *J. Lightw. Technol.*, vol. 32, no. 4, pp. 660–680, 2014.
[9] Y. K. Yeo, J. Yu, and G. K. Chang, "A dynamically reconfigurable foldedpath time delay buffer for optical packet switching," *IEEE Photon. Technol. Lett.*, vol. 16, no. 11, pp. 2559–2561, Nov. 2004.
[10] H. Lee, T. Chen, J. Li, O. Painter, and K. J. Vahala, "Ultra-low-loss optical delay line on a silicon chip," *Nat. Commun.*, vol. 3, no. 867, pp. 1–7, 2012.
[11] A. H. Safavi-Naeini *et al.*, "Electromagnetically induced transparency and slow light with optomechanics," *Nature*, vol. 472, no. 7341, pp. 69–73, 2011.
[12] H.-Y. Tseng, J. Huang, and A. Adibi, "Expansion of the relative time delay by switching between slow and fast light using coherent population oscillation with semiconductors," *Appl. Phys. B*, vol. 85, no. 4, pp. 493–501, 2006.
[13] K. Y. Song and K. Hotate, "25 GHz bandwidth brillouin slow light in optical fibers," *Opt. Lett.*, vol. 32, no. 3, pp. 217–219, 2007.
[14] D. Dahan and G. Eisenstein, "Tunable all optical delay via slow and fast light propagation in a raman assisted fiber optical parametric amplifier: A route to all optical buffering," *Opt. Exp.*, vol. 13, no. 16, pp. 6234–6249, 2005.
[15] H. Takesue, N. Matsuda, E. Kuramochi, W. J. Munro, and M. Notomi, "An on-chip coupled resonator optical waveguide single-photon buffer," *Nat. Commun.*, vol. 4, no. 2725, pp. 1–7, 2013.
[16] F. Leo, S. Coen, P. Kockaert, S. P. Gorza, P. Emplit, and M. Haelterman, "Temporal cavity solitons in one-dimensional kerr media as bits in an all-optical buffer," *Nat. Photon.*, vol. 4, no. 5, pp. 471–476, 2010.
[17] L. Zhuang *et al.*, "Novel low-loss waveguide delay lines using vernier ring resonators for on-chip multi-λ microwave photonic signal processors," *Laser Photon. Rev.*, vol. 7, no. 6, pp. 994–1002, 2013.
[18] F. Morichetti, C. Ferrari, A. Canciamilla, and A. Melloni, "The first decade of coupled resonator optical waveguides: Bringing slow light to applications," *Laser Photon. Rev.*, vol. 6, no. 1, pp. 74–96, 2012.
[19] Q. Xu, S. Sandhu, M. L. Povinelli, J. Shakya, S. Fan, and M. Lipson, "Experimental realization of an on-chip all-optical analogue to electromagnetically induced transparency," *Phys. Rev. Lett.*, vol. 96, no. 12, 2006, Art. no. 123901.
[20] T. Xiaogang, L. Jun, and X. Chenyang, "High-Q micro-ring resonators and grating couplers for silicon-oninsulator integrated photonic circuits," *J. Semicond.*, vol. 34, pp. 0850061– 0850064, 2013.
[21] K. Nozaki *et al.*, "Ultralow-power all-optical RAM based on nanocavities," *Nat. Photon.*, vol. 6, pp. 248–252, 2012.
[22] J. Scheuer and S. Shahriar, "Coupled microrings data buffer using fast light," Spie Opto Int. Soc. for Opt. Photon, vol. 8998, no. 1D, p. 7, 2014.
[23] W. Liu *et al.*, "A wavelength tunable optical buffer based on self-pulsation in an active microring resonator," *J. Lightw. Technol.*, vol. 34, no. 14, pp. 3466–3472, 2016.
[24] K. Ajay, K. Manish, K. J. Sumit, and K. R. Sanjeev, "Implementation of all-optical active low/high tri-state buffer logic using the micro-ring resonator structures," *Opt. Quantum Electron.*, vol. 51, 2019, Art. no. 191.

[25] S. Elshahat, I. Abood, K. Khan, A. Yadav, L. Bibbo, and Z. Ouyang, "Five-line photonic crystal waveguide for optical buffering and data interconnection of picosecond pulse," *J. Lightw. Technol.*, vol. 37, no. 3, pp. 788–798, 2019.
[26] D. Ruzmetov, D. Heiman, B. B. Claflin, V. Narayanamurti, and S. Ramanathan, "Hall carrier density and magnetoresistance measurements in thin-film vanadium dioxide across the metal-insulator transition," *Phys. Rev.*, vol. 79, no. 15, pp. 25–28, 2009.
[27] D. D. Eden, "Some applications involving the semiconductor-to-metal phase transition in VO2," in *Proc. SPIE 0185, Huntsville Tech. Symp. Int. Soc. Opt. Photon.,* 1979.
[28] F. C. Case, "Improved VO_2 thin films for infrared switching," *Appl. Opt.*, vol. 30, no. 28, pp. 4119–4123, 1991.
[29] J. B. Kana, J. M. Ndjaka, G. Vignaud, A. Gibaud, and M. Maaza, "Thermally tunable optical constants of vanadium dioxide thin films measured by spectroscopic ellipsometry," *Opt. Commun.*, vol. 284, no. 3, pp. 807–812, 2011.
[30] B. Chen. "Omnidirectional Infrared Broadband Absorber Based on Multiplexed Metal-Insulator-Metal Structure," M.Sc. thesis, Univ. Buffalo, Fac. Graduate School, 2013.
[31] D. R. Smith, D. C. Vier, T. Koschny, and C. M. Soukoulis, "Electromagnetic parameter retrieval from inhomogeneous metamaterials," *Phys. Rev. e Stat. nonlinear soft matter Phys.*, vol. 71, no. 3, pp. 36617–36610, 2005.
[32] M. J. Dicken *et al.*, "Frequency tunable near-infrared metamaterials based on VO_2 phase transition," *Opt. Exp.*, vol. 17, 2009, Art. no. 18330.
[33] Z. Liu, M. Zhao, J. Gao, Y. Li, and S. JiangLiu, "Thermally tunable broadband omnidirectional and polarization-independent super absorber using phase change material VO_2," *Results Phys.*, vol. 7, 2017, Art. no. 4222.
[34] M. Rini *et al.*, "Optical switching in VO_2 films by below-gap excitation," *Appl. Phys. Lett.*, vol. 92, no. 18, 2008, Art. no. 181904.
[35] K. Appavoo *et al.*, "Ultrafast phase transition via catastrophic phonon collapse driven by plasmonic hot-electron injection," *Nano Lett.*, vol. 14, pp. 127–1133, 2014.
[36] J. N. Caspers, N. Rotenberg, and H. M. van Driel, "Ultrafast silicon-based active plasmonics at telecom wavelengths," *Opt. Exp.*, vol. 18, no. 19, pp. 19761–19769, 2010.
[37] H. K. Yuan, S. C. Chen, L. G. Zhu, Z. H. Zhai, and J. Li, "All optically-controlled multifunctional VO2 memory device for terahertz waves," in *Proc. SPIE 11441 Int. Conf. Opt. Instruments Technol. 2019: IRMMW-THz Technol. Appl. 114410K,* 2020.
[38] A. Melloni *et al.*, "Tunable delay lines in silicon photonics: Coupled resonators and photonic crystals, a comparison," *IEEE Photon. J.*, vol. 2, no. 2, pp. 181–194, Apr. 2010.
[39] H. Kim *et al.*, "Electrical, optical, and structural properties of indium–tin–oxide thin films for organic light-emitting devices," *J. Appl. Phys.*, vol. 86, no. 11, pp. 6451–6461, 1999.
[40] A. Yariv, "Universal relations for coupling of optical power between microresonators and dielectric waveguides," *Electron. Lett.*, vol. 36, 2000, Art. no. 321.
[41] B. E. Little, S. T. Chu, H. A. Haus, J. Foresi, and J. P. Laine, "Microring resonator channel dropping filters," *IEEE J. Lightw. Technol.*, vol. 15, no. 6, pp. 998–1005, Jun. 1997.
[42] M. Ono *et al.*, "Ultrafast and energy-efficient all-optical switching with graphene-loaded deep-subwavelength plasmonic waveguides," *Nat. Photon.*, vol. 14, no. 1, pp. 1–7, 2020.